NEXT-SCALE AUTOREGRESSIVE MODELS ARE ZERO-SHOT SINGLE-IMAGE OBJECT VIEW SYNTHESIZERS

Anonymous authors
Paper under double-blind review

ABSTRACT

Learning to synthesize novel views without explicit 3D representations or hand-crafted 3D inductive bias has recently gained attention: it is simpler, more formally direct, and better aligned with the lesson that scalable learning paradigms with less assumptions built into architectural design (*e.g.*, regarding geometry) often win. However, the current dominant solutions are diffusion-based, which typically suffer from problems like slow inference. We introduce ArchonView, the first autoregressive model for zero-shot single-image, object-centric novel view synthesis (NVS), achieving substantially faster inference, higher accuracies, and notably not relying on fine-tuning of 2D generative checkpoints (challenging the common assumption that 2D priors are required in diffusion-based NVS). We design innovative methods of both global and local conditioning to suit characteristics of the NVS task. Crucially, a naïve application of next-scale autoregression fails; we identify two design choices that unlock performance: local conditioning pre-filling, and removing global AdaLN at the classifier head. ArchonView delivers state-of-the-art zero-shot results across six standard benchmarks (GSO, ABO, OmniObject3D, RTMV, NeRF-Synthetic, ShapeNet), while being several times faster than diffusion baselines (*e.g.*, 0.22s *v.s.* 1.7–1.8s per view at matched parameter count). It consistently improves synthesis accuracy, and scales predictably with both model size (135M–2B) and data size, exhibiting clear scaling-law-like trends. Our findings suggest a paradigm shift and challenge an existing assumption: first, for object-centric NVS, next-scale autoregression can be faster, simpler, and more accurate than diffusion; and second, priors obtained from fine-tuning 2D-pretrained models may not be necessary for generative NVS. Our code is open-sourced at `https://anonymous.4open.science/r/ArchonView/`.

1 INTRODUCTION

Humans, living in a 3D world, naturally infer the complete 3D structure of objects from a single 2D view, leveraging prior knowledge and spatial reasoning. If machines could achieve the same, particularly in a zero-shot manner for unseen objects, it would greatly benefit fields such as 3D content creation, simulation, and real-world perception systems. Consequently, zero-shot novel view synthesis (NVS) from single object-centric images emerges as a fundamental challenge in computer vision. Since this is a highly under-constrained problem, it is typically formulated as a generative task conditioned on the input image and relative camera pose. The prevailing approach fine-tunes a 2D diffusion model to exploit implicit geometric priors learned from large-scale image datasets. Whilst this paradigm has shown promising results, it comes with several limitations.

A critical limitation of diffusion models is their inherent trade-off between speed and quality. Due to the need for multiple denoising steps through a U-Net structure, achieving high-quality outputs inevitably results in relatively slow inference. Consequently, if diffusion models were scalable, larger models would further increase inference time and computational cost, potentially rendering them impractical for real-world deployment. Furthermore, notably, to the best of our knowledge, no prior work has demonstrated scaling trends with respect to model size for single-image object-centric NVS. We consider this to perhaps be attributable to a previous common assumption, introduced in works like Liu et al. (2023), which conclude that 2D priors obtained from fine-tuning pretrained 2D generative models (such as Stable Diffusion) are necessary for zero-shot NVS. Since it is impossible for most researchers to train a 2D generative model from scratch, this has limited most current

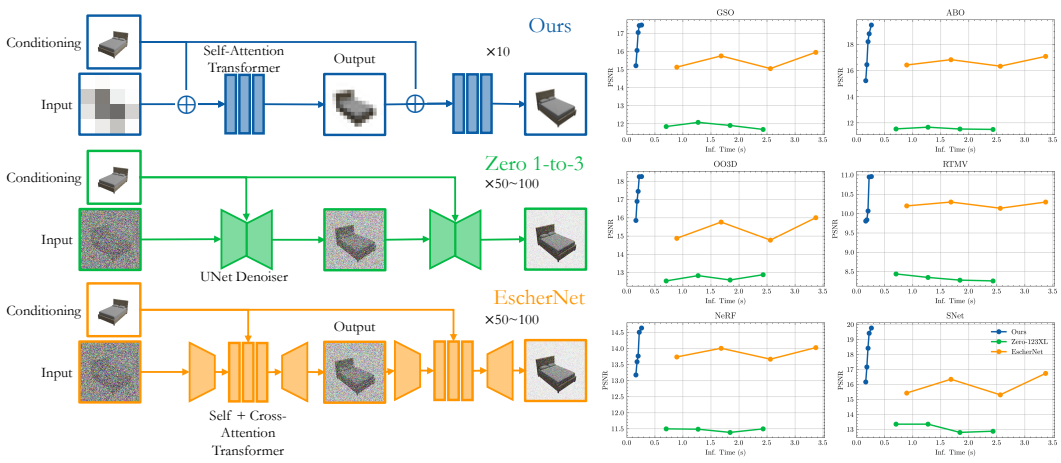

Figure 1: **Fast, accurate, and scalable novel view synthesis without fine-tuning.** We achieve better results via paradigm shift, by using an autoregressive scheme to replace previous diffusion schemes. The left shows the abstract architecture of each autoregression/diffusion step. On the right are time *v.s.* PSNR tradeoff plots, where our models scaled to different parameter sizes are compared against diffusion models with different denoising steps.

models to be based on fine-tuning Stable Diffusion, and hence remaining at the size of around 1.0B parameters.

We explore the potential for a paradigm shift: a backbone architecture which can be readily scaled up, does not require 2D pretraining, is more efficient, and outputs better results. To this end we propose Autoregression Conditioned by View (ArchonView), the first NVS model based on visual autoregressive generation. We base our method on the recently proposed next-scale autoregression backbone, which replaces raster-scan-ordered next-token prediction in conventional visual autoregression with autoregressively predicting the next resolution scale of tokens in a coarse-to-fine manner (described in Sec. 3.2). Whilst previous works have verified its scalability and applicability to many tasks in vision, so far, its applicability to NVS remains unknown.

In order to adapt autoregression to NVS, we condition the model in two ways: globally, through a posed CLIP encoding, which allows the model to gain semantic information augmented by the desired relative pose (described in Sec. 3.3); and locally, encoded by the multiscale VQVAE representation (which is also used for quantization in the main generative architecture), enforcing consistency in local details with the input image (described in Sec. 3.4). Experimentation shows that our method achieves state-of-the-art performance consistently and robustly across multiple benchmarks, scales with both model size and dataset size, and is several times faster than current diffusion-based methods. Some of our results across different evaluation datasets and comparisons with current methods are shown in Fig. 1.

In summary, our key technical contributions to the field of zero-shot single-image object NVS are as follows:

- We present a method that consistently achieves state-of-the-art performance and is also several times faster in terms of inference time compared to previous works.
- Our method does not require fine-tuning on a 2D generative model, and hence challenges the existing assumption that pretrained 2D priors are necessary for zero-shot capability in generative NVS.
- We demonstrate that our method scales with both model size and dataset size.
- We are the first to base a model on an autoregressive backbone for this task, demonstrating the potentials of next-scale autoregression.

2 Related Works

2.1 Generative Modeling

Autoregression has seen many applications to generation of language (Brown et al., 2020; Radford et al., 2018; 2019; Touvron et al., 2023), world models (Bruce et al., 2024; Lu et al., 2024; Tu

et al., 2025), videos (Kondratyuk et al., 2024; Wu et al., 2022; Yan et al., 2021), and multimodal outputs (Chameleon Team, 2024; Kelly et al., 2024; OpenAI, 2023; Sun et al., 2023). Besides being efficient and accurate enough for operational use, it has also been shown to be scalable in many tasks (Henighan et al., 2020; Kaplan et al., 2020). However, the current predominant paradigm of 2D generative modeling is indubitably diffusion, thanks to multiple groundbreaking innovations in this field (Ho & Salimans, 2021; Peebles & Xie, 2023; Rombach et al., 2022; Zhang et al., 2023). Meanwhile, though conventional visual autoregression (using a raster-scan traversal of fixed-size patches as tokens) has produced innovative techniques (Esser et al., 2021; Lee et al., 2022; Parmar et al., 2018; Van Den Oord et al., 2017; Yu et al., 2022a) and achieved some milestones (Chen et al., 2020; Ramesh et al., 2021; Razavi et al., 2019; Yu et al., 2022b), advances in diffusion left it largely irrelevant.

Recently, the newly proposed next-scale prediction paradigm of autoregression (Tian et al., 2024), replacing the conventional raster-scan next-token paradigm, has been proven effective, developed upon (Gu et al., 2024; Ren et al., 2024a;b; Tang et al., 2025), and adapted (Han et al., 2024; Li et al., 2024; 2025; Ma et al., 2024; Yao et al., 2024). Empirical evidence demonstrates its reliability in achieving accurate, efficient, and scalable results, exceeding diffusion models in many tasks where raster-scan autoregression struggles. This has reignited interest in using autoregressive models for visual generative tasks where diffusion models currently dominate.

2.2 Novel View Synthesis

Before the advent of generative NVS models, predominant methodologies have used implicit representations (Barron et al., 2021; 2022; 2023; Mildenhall et al., 2021), voxel-like representations (Chen et al., 2022; Fridovich-Keil et al., 2022; Sun et al., 2022; Yu et al., 2021a), explicit primitives (Huang et al., 2024; Kerbl et al., 2023; Mai et al., 2024; Müller et al., 2022), *etc.* to model 3D scenes or objects based on given views and poses, thus achieving NVS. However, in the case of sparse inputs, where few views or only one view is available, none of those models are able to produce accurate results due to the scene being severely underconstrained.

While some efforts have been made to adapt conventional frameworks to sparse-input scenarios (Chen et al., 2021; Chibane et al., 2021; Jain et al., 2021; Niemeyer et al., 2022; Xu et al., 2022; Yu et al., 2021b), their capabilities were limited, or often depended on strict hypotheses regarding geometrical priors. In addition, most aforementioned methods require specific training or fine-tuning on the scene or object in question, or were fine-tuned on a class of objects (*e.g.*, from ShapeNet (Chang et al., 2015)) and only perform well for in-distribution inputs. Thus, none achieved capability for zero-shot single-image NVS with such paradigms.

2.3 Generative NVS

Early works have used GANs (Goodfellow et al., 2014) as backbones for conducting NVS generatively, reframing the problem as modeling the distribution of scene views conditioned by camera pose (Chan et al., 2021; 2022; Gadelha et al., 2017; Nguyen-Phuoc et al., 2019; Niemeyer & Geiger, 2021; Schwarz et al., 2022). In late 2022 through 2023 there was a surge of works using diffusion models for NVS, often coupled with the then-recent NVS representations (*e.g.* NeRF); in particular, some works used diffusion models as priors for supervising the training of a 3D representation model (Bautista et al., 2022; Deng et al., 2023; Melas-Kyriazi et al., 2023; Sargent et al., 2024; Wang et al., 2023; Wu et al., 2024), while others directly used diffusion models with camera pose conditioning as an NVS representation backbone (Chan et al., 2023; Liu et al., 2023; Watson et al., 2023) (interestingly the latter's methodology of view generation based on latents coincides with previous works using transformers (Kulhánek et al., 2022; Rombach et al., 2021; Sajjadi et al., 2022)).

A particularly important work in this period was Zero 1-to-3 (Liu et al., 2023), which was fine-tuned on an image variation model (Pinkney, 2023) which, in turn, was tuned on Stable Diffusion (Rombach et al., 2022). Its main conclusion was that 2D diffusion models already contain 3D-aware priors, and that such priors can be directly extracted by fine-tuning pretrained 2D diffusion checkpoints. This paradigm of fine-tuning 2D diffusion models for priors spawned a line of works (Kong et al., 2024; Liu et al., 2024; Shi et al., 2023; Watson et al., 2024; Ye et al., 2024; Zheng & Vedaldi, 2024) which similarly attempt to extract 3D-aware priors from pretrained 2D diffusion models.

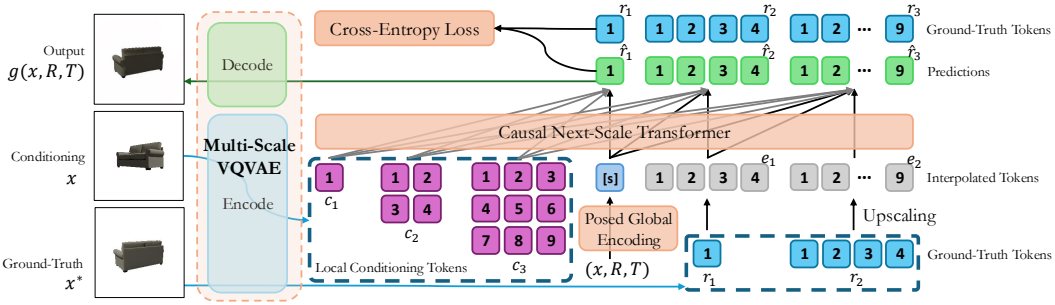

Figure 2: **The overall architecture for the training of ArchonView.** The predictions are classifier logit predictions, and can be converted to images after sampling based on the logit probabilities. The loss calculation is directly based on the logits and does not involve sampling.

2.4 Our Contribution

In our work, we demonstrate that autoregressive models can directly possess 3D-awareness without relying on checkpoints from 2D pretraining, differing from the conclusion of Zero 1-to-3. We also show that the autoregressive paradigm can be superior to its diffusion-based counterpart in terms of both speed and accuracy. We note that some very recent concurrent works (Kong et al., 2025; Nair et al., 2025) have also noticed the potential of transformer architectures in the task of NVS in general, but still rely on pretrained diffusion models as backbone for generation. We are the first work to show that in fact, autoregression is all one needs, and that neither diffusion nor fine-tuning are necessary. On top of this, our model achieves a very high increase in accuracy and efficiency compared to diffusion, suggesting that next-scale autoregression may be better suited to the task of zero-shot single-image NVS. The natural scalability of our model also provides it with high potential for applicational use.

We also note that there exists an adjacent line of works which directly produce 3D models of objects from a single image (Hong et al., 2024; Tang et al., 2024; Xiang et al., 2025; Zhang et al., 2025). However, as was pointed out by many previous works (Jin et al., 2025; Zheng & Vedaldi, 2024), models that explicitly maintain an underlying 3D representation sacrifice underlying NVS accuracy and efficiency considerably. While a lot of progress has been achieved in this direction, so far no image-to-3D model can directly achieve NVS performance better than pure NVS models.

3 Methodology

3.1 Motivation

Problem Formulation Formally, we wish to solve the following problem. Given a single input view x of an underlying 3D object, as well as relative camera transformations $R \in \mathbb{R}^{3\times3}$ and $T \in \mathbb{R}^3$, we would like to create a probabilistic model $g(x, R, T)$ such that the output view

$$x^*_{R,T} \sim g(x, R, T) \tag{1}$$

follows the distribution of the transformed view from applying the relative camera transformation (R, T) on x.

Diffusion is Not All You Need The current predominant formulation of our problem is as a diffusion model. Specifically, common architectures based on the latent diffusion paradigm (Rombach et al., 2022) are made up of an image encoder-decoder pair $(\mathcal{E}, \mathcal{D})$, a U-Net denoiser ϵ_θ, and a conditioning encoder τ. The latents $z \sim \mathcal{E}(x)$ are then corrupted with additive Gaussian noise at each step, forming noised latents z_t. Diffusion models are thus trained based on the objective

$$\min_\theta \mathbb{E}_{z\sim\mathcal{E}(x),\epsilon\sim\mathcal{N}(0,1),t}||\epsilon - \epsilon_\theta(z_t, t, \tau(x, R, T))||_2^2. \tag{2}$$

However, we notice a key downside of this formulation; zero-shot capabilities in this line of research are dependent upon priors within 2D pretrained diffusion models. For instance, one can compare (Watson et al., 2023) with (Liu et al., 2023), which are both based on the presented model; the former was not tuned from 2D models and thus did not exhibit zero-shot abilities, while the latter was tuned from Stable Diffusion and used CLIP for conditioning encoding, thus allowing

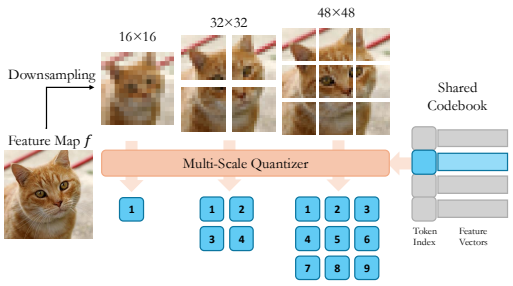

Figure 3: **Structure of the multi-scale VQ-VAE.** The VQVAE converts the input image into a feature map, resizing it into different scales, and using a codebook shared between scales to compress the patches.

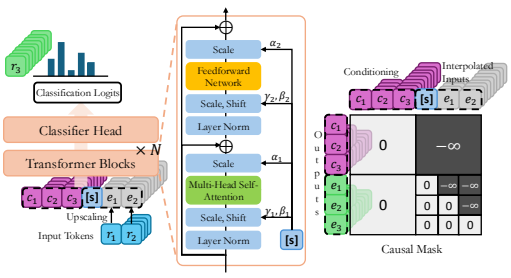

Figure 4: **The next-scale prediction transformer architecture.** Next-scale prediction passes local conditioning tokens and input tokens through multiple transformer blocks (with masking) which are conditioned by adaptive layer normalization.

zero-shot NVS. This naturally leads to a scalability issue: since the underlying checkpoints require large amounts of data and computation to train, it is difficult to scale existing models up. To the best of our knowledge, most or potentially all works in this direction are tuned from Stable Diffusion. Diffusion models also have other problems such as relatively slow inference speed (due to repeated denoising passes), which further limit their effectiveness.

3.2 Backbone Architecture

We propose using next-scale autoregression as our backbone paradigm instead and modifying it to suit our task. Our overall architecture during training is shown in Fig. 2. Next-scale autoregression is based on predicting the next resolution scale of the image in a coarse-to-fine manner, and consists of two main parts: a multi-scale vector-quantized variational autoencoder (VQVAE) (Van Den Oord et al., 2017) which supports image tokenization (depicted in Fig. 3), and a transformer which autoregressively predicts the next scale of tokens (depicted in Fig. 4). More details regarding the implementation those two components can be found in App. C. Here, we emphasize our main innovations in design to adapt the paradigm specifically for our task of NVS:

Adding Local Conditioning While there are many tried-and-true methods regarding autoregression conditioning, we note that many of them do not fit our case. For instance, Li et al. (2025), using conventional autoregression, fuses conditioning and input tokens to achieve high efficiency and quality in generation. However, their fundamental logic does not trivially extend to novel-view synthesis: in most generative tasks (*e.g.*, sketch-to-paint, canny edge-conditioned generation, segmentation-conditioned generation), patches at the same positions in an image correspond closely to each other. However, in novel view synthesis, the correspondence between patches depends entirely on the camera pose desired, and hence this correspondence is broken. A demonstration of this phenonmenon for NVS is shown in Fig. 5.

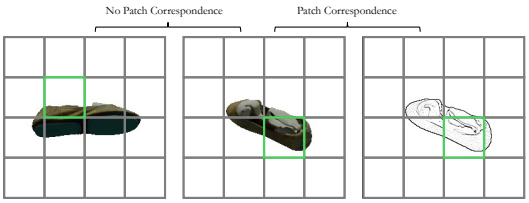

Figure 5: **Demonstration of the failure of patch correspondence.** A conditioning image and its ground-truth canny edge contain highly correlated features at patches of the same location. A conditioning image and its ground-truth novel view may have almost unrelated visual features, and even corresponding parts of the object in the image are usually in patches at different locations.

To solve this problem, we tried multiple architectures to find the most suitable conditioning for this purpose. Visualizations of their schemes are shown in Fig. 6. These include the classical prefilling, causal conditioning, and using cross-attention to fuse corresponding conditioning and input tokens of the same scale. Causal conditioning is inspired by works like Li et al. (2024), where conditioning tokens are causally masked in the same way as their corresponding input tokens of the same scale. Cross-attention (with conditioning tokens as key and value, and input tokens as key) is a variation on the idea of fusing corresponding tokens (Li et al., 2025): due to broken patch-to-patch correspon-

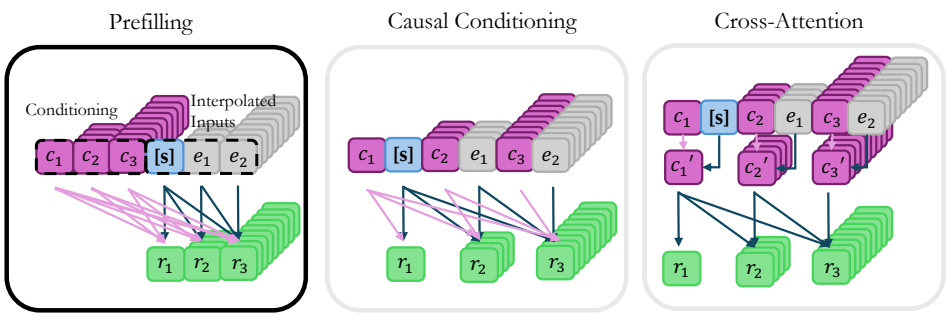

Figure 6: **Autoregressive conditioning schemes we tested.** The one that we chose (and presented in Fig. 2) was Prefilling.

dence, we instead let cross-attention automatically produce correspondences between patches of the same scale.

Results of preliminary tests show that simple prefilling turns out to exceed the other two methods by wide margins. This gives two insights into the mechanism of generative NVS. First, this means that causality between the conditioning image and the generated tokens is no longer single-direction next-scale dependency, and hence that connections from higher-resolution conditioning to lower-resolution outputs are needed. Second, this shows fusing conditional and input tokens is no longer an effective method due to correspondences being broken, even when we use more sophisticated methods than simple concatenation.

The Devil is in the Classifier Head We identify a seemingly innocuous and intuitive implementation feature that was not mentioned in the paper introducing next-scale autoregression (Tian et al., 2024), but turned out to be fatally detrimental to our task (as verified by our ablation studies presented in Sec. 4.2). The original implementation of the next-scale transformer applies adaptive normalization before the classifier head, which would seem as very natural and harmless, as all transformer layers also had adaptive normalization and indeed benefited from it. However, we found that in our task this significantly restricts the performance of the resulting model considerably. Removing this unleashed a significant performance improvement for our model.

We theorize that this implies global conditioning using AdaLN must be accompanied by self-attention with local conditioning tokens (as the classification logit prediction step does not involve attention transformers), and that otherwise only using global conditioning would prompt the output image to "forget" details from local conditioning. Specifically, the scale and shift for this AdaLN were derived from a linear layer, and hence are shared across all inputs, which seems irrational given the highly pose-conditioning-dependent nature of the NVS task.

3.3 Semantic Global Pose Conditioning

We now start presenting the details of how we adapted the architecture via adding conditioning for our task. Firstly, we need to choose a start token that reliably captures global information from our conditioning (x, R, T), because it will be used both for initializing the autoregressive procedure and for normalization of every attention layer, which means it should have complete field of view. Meanwhile, it must also be a single token because it will be mapped to the first resolution scale (which comprises of a single patch) during autoregressive inference.

To balance those two needs, we would like an encoding scheme that could condense semantic information from the image along with the query poses into a vector of size comparable to tokens. Inspired by Liu et al. (2023), we use a "Posed CLIP" embedding as follows:

$$\tau(x, R, T) = W(W_i(\text{CLIP}(x) \oplus [\theta, \sin\phi, \cos\phi, r]) + b_i) + b. \tag{3}$$

Here, θ, ϕ, and r respectively stand for the relative elevation, azimuth, and radial distance of the transformation; $\oplus$ stands for concatenation along the feature dimension; $\text{CLIP}(x) \in \mathbb{R}^{768}$ is the CLIP visual embedding (Radford et al., 2021), which we use here as a global semantic encoder; and $(W_i, b_i), (W, b)$ are two pairs of linear layer parameters, where the i subscript stands for identity initialization (*i.e.* W_i is initialized as an identity matrix and b is initialized as a zero vector).

The two layers here serve different purposes. The identity-initialized layer $W_i \in \mathbb{R}^{768\times772}, b_i \in \mathbb{R}^{768}$ aims to merge the relative pose information into the original CLIP features. The other layer

Table 1: **Quantitative benchmarking results.** We compare against state-of-the-art baselines using diffusion backbones on six well-established benchmarking datasets.

	GSO			ABO			OO3D			
	PSNR (↑)	SSIM (↑)	LPIPS (↓)	PSNR (↑)	SSIM (↑)	LPIPS (↓)	PSNR (↑)	SSIM (↑)	LPIPS (↓)	Time (s)
Zero 1-to-3	13.39	0.7776	0.2672	12.75	0.7632	0.2901	13.43	0.7737	0.2723	1.84
Zero 123-XL	13.80	0.7865	0.2595	12.78	0.7646	0.2766	14.05	0.7966	0.2516	1.84
EscherNet	16.77	0.8275	0.1891	17.03	0.8381	0.1693	16.12	0.8294	0.2060	1.68
Ours	**17.44**	**0.8491**	**0.1853**	**18.82**	**0.8725**	**0.1360**	**18.26**	**0.8622**	**0.1617**	**0.22**
	RTMV			**NeRF**			**SNet**			
	PSNR (↑)	SSIM (↑)	LPIPS (↓)	PSNR (↑)	SSIM (↑)	LPIPS (↓)	PSNR (↑)	SSIM (↑)	LPIPS (↓)	Params
Zero 1-to-3	8.49	0.5260	0.4772	10.88	0.6222	0.4146	13.02	0.7957	0.3288	1.0B
Zero 123-XL	8.58	0.5237	0.4735	11.29	0.6551	0.3926	13.29	0.8070	0.3206	1.0B
EscherNet	10.38	0.5327	0.4340	13.85	0.6783	0.2868	16.35	0.8450	0.1951	1.0B
Ours	**10.95**	**0.5739**	**0.3991**	**14.51**	**0.7025**	**0.2735**	**19.42**	**0.8927**	**0.1300**	**1.0B**

Table 2: **Ablation study results.** We evaluate the necessity of two design choices: adding local conditioning (as in Sec. 3.4), and removing adaptive layer normalization for the classifier head.

	GSO			ABO			OO3D		
	PSNR (↑)	SSIM (↑)	LPIPS (↓)	PSNR (↑)	SSIM (↑)	LPIPS (↓)	PSNR (↑)	SSIM (↑)	LPIPS (↓)
Global Only	13.25	0.7959	0.2672	13.04	0.7892	0.3116	15.03	0.8161	0.2523
w/ Cls. Head AdaLN	12.76	0.7885	0.2510	12.80	0.7549	0.3131	12.59	0.7832	0.2540
Ours	**17.44**	**0.8491**	**0.1853**	**18.82**	**0.8725**	**0.1360**	**18.26**	**0.8622**	**0.1617**
	RTMV			**NeRF**			**SNet**		
	PSNR (↑)	SSIM (↑)	LPIPS (↓)	PSNR (↑)	SSIM (↑)	LPIPS (↓)	PSNR (↑)	SSIM (↑)	LPIPS (↓)
Global Only	8.74	0.4968	0.5124	11.80	0.6280	0.4176	14.52	0.8232	0.2906
w/ Cls. Head AdaLN	7.39	0.4771	0.5301	10.41	0.5958	0.4237	12.73	0.7929	0.2739
Ours	**10.95**	**0.5739**	**0.3991**	**14.51**	**0.7025**	**0.2735**	**19.42**	**0.8927**	**0.1300**

$W \in \mathbb{R}^{C\times 768}, b \in \mathbb{R}^C$, initialized normally, serves as an interface between the semantic embedding and the transformer architecture by mapping it onto a token. The (W_i, b_i) layer is set to have 10 times the learning rate of other parameters, as in our experiments without this setting the gradient quickly explodes, which shows that this layer is an important information bottleneck.

We add classifier-free guidance (CFG) by randomly replacing values in the 768-dimensional posed CLIP embedding with values from a null CLIP text embedding (applying the CLIP text encoder to an empty string). This ensures that we are able to continue enjoying benefits brought by diffusion models' CFG in strengthening the impact of pose conditioning.

3.4 Multi-Scale Local Conditioning

The global encoding is a good condition for generation because it aggregates semantic information across the entire image and has full field-of-view. However, in this process, the details of the original image are lost. Hence we need to add another source of conditioning which can directly provide the autoregressive model with portions of the input image. To this end we propose a local conditioning mechanism to provide effective conditioning information for the attention layers.

As previously shown in Fig. 2, we encode the conditioning image x through the multi-scale VQVAE into tokens the same way as we encode the ground-truth x^*. This ensures that the conditioning tokens and tokens used during generation share the same vocabulary (from the VQVAE codebook Z), thus facilitating the application of self-attention in the next-scale transformer.

We extend the block triangular mask such that all conditioning tokens can affect the next attention block's conditioning and the input tokens, but are not affected by input tokens (as displayed in Fig. 4). This method of conditioning via token prepending is well-suited to the autoregressive nature of our paradigm, and does not require any architectural accommodations. We observe in our ablation studies that this greatly enhances the effectiveness of our method compared to purely using a global encoding as conditioning. We add classifier-free guidance by randomly replacing local conditioning tokens with a learnable null token.

In conventional diffusion-based methods, the predominant way of adding local conditioning is to channel-concatenate the conditioning image onto the latent noise used for diffusion. However, as previous works have noted (Shi et al., 2023), this inherently creates a false pixel-to-pixel correspondence between the conditioning image and the latent whereas the actual relationship is a lot more non-trivial (as transformations in 3D are involved). Our method, in contrast, does not inherently impose any correspondences. Since the multi-scale encoding is inherently hierarchical, not only can the transformer learn correspondence relationships without any structural assumptions, it can

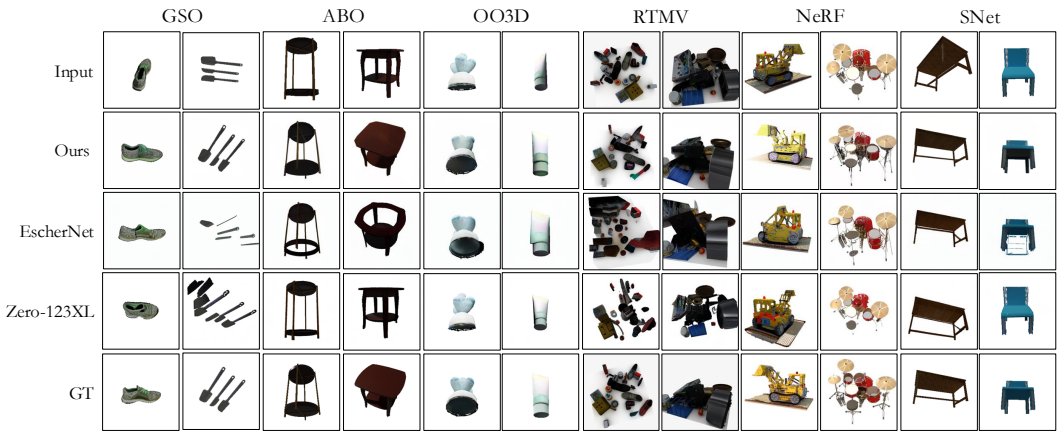

Figure 7: **Qualitative results.** Visual comparisons of our method with diffusion-based prior works.

also model more complex relationships that require information from several levels of detail. This also allows for emergent aggregation of information, as our visualization of attention maps later confirms.

4 Experiments

4.1 Settings

Training We use the multi-scale VQVAE checkpoint from Tian et al. (2024), which was trained on the OpenImages dataset (Kuznetsova et al., 2020). We train our models on the Objaverse dataset (Deitke et al., 2023), from which we render 256×256 views with randomly sampled camera poses. The number of 16×16 patches per side for each VQVAE scale follows the progression $(1, 2, 3, 4, 5, 6, 8, 10, 13, 16)$, for a total of 10 prediction steps. The depth of the model is set to be 24 for benchmarking in order for the model size to be 1.0B, matching diffusion-based baselines. More training details are described in App. B.

Evaluation We conduct evaluation across six common datasets: Google Scanned Objects (GSO) (Downs et al., 2022), Amazon Berkeley Objects (ABO) (Collins et al., 2022), OmniObject3D (OO3D) (Wu et al., 2023), Ray-Traced Multi-View Synthetic (RTMV) (Tremblay et al., 2022), NeRF Synthetic (NeRF) (Mildenhall et al., 2021), and ShapeNet Core (SNet) (Chang et al., 2015). None of those datasets overlap with our training set (Objaverse), which means that all of the experimental results are zero-shot inference. To the best of our knowledge, this is the most comprehensive evaluation set (in terms of the number of independent datasets used) assembled in our line of work. Unlike previous works which, for unknown reasons, have standardized using an evaluation setting easier than the training setting, we use an evaluation setting that is the same as the training setting to test model robustness, detailed in App. A.

4.2 Results

Benchmarking Quantitative results from our benchmarking are shown in Tab. 1. As shown, our model, while being of the same size as the Stable Diffusion-tuned baselines, is up to more than 8 times faster than those baselines (under their officially recommended settings), and consistently produces significantly better results across our 6 vastly distinct benchmarks.

Qualitative Comparison We present qualitative results in Fig. 7. As shown, our model produces more accurate reconstructions, and also can achieve more realistic and feasible results (*e.g.*, GSO shoe) even though it has seen far fewer visual information than the diffusion-based baselines (which have gone through 2D pretraining). Furthermore, our model is also good at localizing objects after transformation even in cluttered scenes (*e.g.*, RTMV), and has a good understanding of geometrical structure (*e.g.*, SNet table). Even when outputs are inaccurate due to uncertainty regarding factors such as lighting (*e.g.*, NeRF lego bulldozer), it continues to present accurate geometries and feasible lighting/texture. Surprisingly, although one might expect diffusion-based models would be more capable of predicting unseen portions of objects due to its knowledge of 2D priors, it seems that

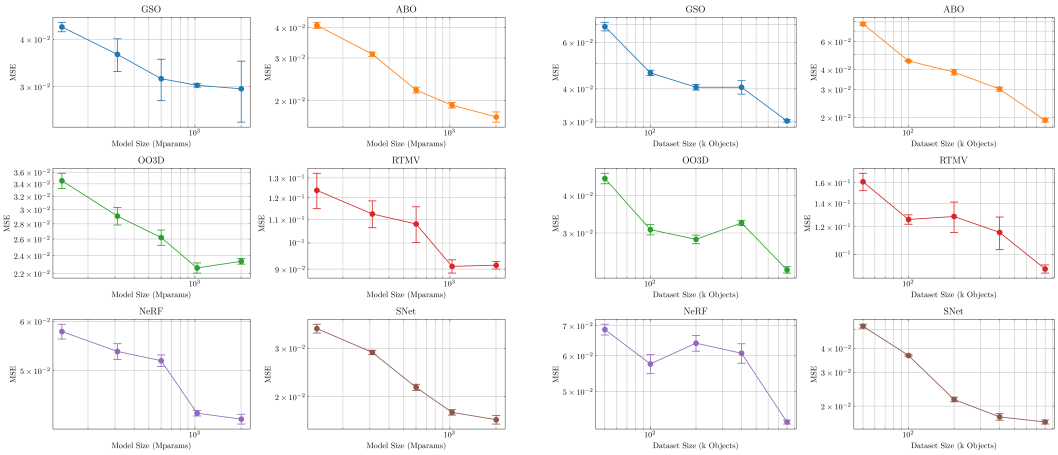

(a) **ArchonView scaling with model size.** The five tested models have depth 12, 16, 20, 24, and 30.

(b) **ArchonView scaling with dataset size.** We randomly subsample subsets from our training set.

Figure 8: **Scaling behavior we observed from Archonview.** Error bars are ± one standard deviation from five repetitions each.

ours often better (*e.g.*, ABO — note how EscherNet creates counterintuitive holes and Zero-123XL struggles to change viewpoints correctly). This supports our hypothesis that priors obtained from fine-tuning 2D generative models may not be necessary.

Ablation We compare our model with a version that uses only global encodings, and one that keeps AdaLN with its classifier head. The results in Tab. 2 show that both of the tested design choices were necessary for the model to achieve acceptable results. This shows that our local embedding effectively encodes local features, enabling our model to synthesize high-quality and precise novel views. In addition, this verifies our assessment on the effect of AdaLN on the classifier head, proving that local conditioning is always necessary after global conditioning to prevent loss of information.

Scaling We investigate the model's scaling behavior with respect to model size and dataset size (we do not consider scaling with computation due to the difficulty of rigorously defining an optimal stopping point, as in our case performance is not directly tied to token accuracy unlike in other tasks like LLMs). Results are shown in Figs. 8a and 8b. It seems that adding more data would likely continue to improve model performance considerably. As for model size, results demonstrate preliminary evidence of scaling law-like behavior below 1B parameters, and the performance of larger models is likely bottlenecked by dataset size. We expect the scaling behavior to hold when data, model size, and training compute are scaled up simultaneously, although a necessary limit will be imposed by entropy from the uncertainty of unseen parts.

Zero-Shot Spatial Understanding In order to demonstrate that our models has indeed acquired the ability of zero-shot spatial understanding, we visualize the attention maps of conditioning tokens in 9. The heatmap represents how much information each token in the resulting image draws from the conditioning token, and bases it on averaging the attention scores over each of the heads and layers. The results show a clear pattern: output tokens spatially or semantically related to the input token tend to have higher attention scores. Notably, a patch of the white background always corresponds to the boundary of the object, showing global geometric understanding. Tokens surrounding the input token in 2D space also tend to have higher attention scores, which is because the next-scale approach naturally clusters local information onto appropriate places in pixel space. The results support that our model has meaningful emergent capability for 3D-aware spatial understanding and information aggregation.

5 Discussion

According to Liu et al. (2023), diffusion-based object-centric NVS models work by adapting visual priors inherent in pretrained 2D diffusion models. This, in turn, causes heavy reliance on large pretrained models such as Stable Diffusion (which was trained on over 2B images (Schuhmann et al., 2022)). In contrast, we only use the "fine-tuning" dataset of previous works (with 800k 3D objects)

Figure 9: **Demonstration of emergent zero-shot spatial understanding capabilities.** Each of the images on the left are the conditioning images, and the image on the right is the target image for reference. The red-highlighted patch on the left corresponds to the conditioning token we choose, and the heatmap shows its attention map.

and achieved significantly superior results. This demonstrates that under the autoregressive formulation, the 3D objects already contain enough information for the model to accurately, efficiently, and scalably conduct object-centric NVS. Furthermore, trends in Fig. 8b show that increasing the dataset size beyond 800k (Objaverse) is likely to yield further positive results, which gives a clear direction for the next step of scaling ArchonView towards operational usage.

By using an autoregressive paradigm, we also avoid blurry output that defy prior knowledge of real-life objects which often occur in diffusion models, as unlike diffusion models which are continuous, the discrete representation enforced by the codebook directly filters out cases with low prior probability. This is beneficial for output fidelity and visual quality.

In addition, our superior speed and accuracy suggests the potential for a paradigm shift from diffusion to next-scale autoregression in the field of generative NVS, which avoids diffusion's "original sins" in speed and scalability that stem from the need for repeated denoising steps. Next-scale autoregression is also a rapidly evolving technique, and many advances in this line of research can possibly be used as plug-in improvements to our method. Hence we believe ArchonView can function as a base model for future innovations that can further drive this paradigm shift.

While our work aims to mainly explore the possibility of a paradigm shift and thus focused on the more fundamental task of NVS, we believe that our methodology can be easily modified to suit other downstream tasks. A particularly hopeful direction for future research is applying our method to 3D generation. This can be done by adopting a multi-view paradigm, as is common in current diffusion-dominated literature, such that consistency can be emergently imposed, facilitating conversion into 3D representations such as NeRFs, Gaussian splats, and meshes.

6 Conclusion

We introduce the first method of zero-shot single-image object-centric NVS to be based on visual autoregression, using the next-scale autoregression paradigm. We show that it does not require fine-tuning on 2D-pretrained checkpoints, achieves state-of-the-art performance across several benchmark tasks, is several times faster in inference time compared to previous methods, and demonstrates scaling behavior with model size and dataset size. This demonstrates the oft-overlooked potential of autoregressive backbones and their advantages over diffusion for NVS tasks, and provides a base model for potential future work in this direction.

Our main conclusions on the theoretical implications are: autoregression as a backbone paradigm for generative NVS may be more suitable than diffusion (in terms of accuracy and speed); differing from previous consensus, priors from 2D generation may not be necessary for generative NVS; and that scaling laws are expected to hold for generative NVS models with suitable architecture, as was shown for our design. We hope future work can derive more meaningful insights from our reframing of the problem.

Ethics Statement

Results presented by this work, given their visual generative nature, are prone to being exploited by malicious agents. We encourage responsible usage in accordance with relevant common guidelines. The "Direct Use" portion of the DALL-E Mini model card (OpenAI, 2022), shared by works such as Stable Diffusion (Rombach et al., 2022), applies well.

Reproducibility Statement

The code repository we provide in the abstract provides everything one needs to reproduce our results to their exact values (all random components were seeded as well to ensure this). This includes all used checkpoints, the training/validation/evaluation sets (already rendered and paired with pre-computed CLIP embeddings for the reader's convenience), the training/inference code, and package requirements. **We strongly encourage readers to try out our code.** Note that while Anonymous GitHub sometimes shows "The requested file is not found," this does not seem to affect downloading the repository.

References

Jonathan T Barron, Ben Mildenhall, Matthew Tancik, Peter Hedman, Ricardo Martin-Brualla, and Pratul P Srinivasan. Mip-NeRF: A Multiscale Representation for Anti-Aliasing Neural Radiance Fields. In *Proceedings of the IEEE/CVF International Conference on Computer Vision*, pp. 5855–5864, 2021.

Jonathan T Barron, Ben Mildenhall, Dor Verbin, Pratul P Srinivasan, and Peter Hedman. Mip-NeRF 360: Unbounded Anti-Aliased Neural Radiance Fields. In *Proceedings of the IEEE/CVF Conference on Computer Vision and Pattern Recognition*, pp. 5470–5479, 2022.

Jonathan T Barron, Ben Mildenhall, Dor Verbin, Pratul P Srinivasan, and Peter Hedman. Zip-NeRF: Anti-Aliased Grid-Based Neural Radiance Fields. In *Proceedings of the IEEE/CVF International Conference on Computer Vision*, pp. 19697–19705, 2023.

Miguel Angel Bautista, Pengsheng Guo, Samira Abnar, Walter Talbott, Alexander Toshev, Zhuoyuan Chen, Laurent Dinh, Shuangfei Zhai, Hanlin Goh, Daniel Ulbricht, Afshin Dehghan, and Josh Susskind. GAUDI: A Neural Architect for Immersive 3D Scene Generation. *Advances in Neural Information Processing Systems*, 36:25102–25116, 2022.

Tom B Brown, Benjamin Mann, Nick Ryder, Melanie Subbiah, Jared Kaplan, Prafulla Dhariwal, Arvind Neelakantan, Pranav Shyam, Girish Sastry, Amanda Askell, Sandhini Agarwal, Ariel Herbert-Voss, Gretchen Krueger, Tom Henighan, Rewon Child, Aditya Ramesh, Daniel M Ziegler, Jeffrey Wu, Clemens Winter, Christopher Hesse, Mark Chen, Eric Sigler, Mateusz Litwin, Scott Gray, Benjamin Chess, Jack Clark, Christopher Berner, Sam McCandlish, Alec Radford, Ilya Sutskever, and Dario Amodei. Language Models are Few-Shot Learners. *Advances in Neural Information Processing Systems*, 34, 2020.

Jake Bruce, Michael D Dennis, Ashley Edwards, Jack Parker-Holder, Yuge Shi, Edward Hughes, Matthew Lai, Aditi Mavalankar, Richie Steigerwald, Chris Apps, Yusuf Aytar, Sarah Bechtle, Feryal Behbahani, Stephanie Chan, Nicholas Heess, Lucy Gonzalez, Simon Osindero, Sherjil Ozair, Scott Reed, Jingwei Zhang, Konrad Zolna, Jeff Clune, Nando de Freitas, Satinder Singh, and Tim Rocktäschel. Genie: Generative Interactive Environments. In *International Conference on Machine Learning*, 2024.

Chameleon Team. Chameleon: Mixed-Modal Early-Fusion Foundation Models. *arXiv preprint arXiv:2405.09818*, 2024.

Eric R Chan, Marco Monteiro, Petr Kellnhofer, Jiajun Wu, and Gordon Wetzstein. pi-GAN: Periodic Implicit Generative Adversarial Networks for 3D-Aware Image Synthesis. In *Proceedings of the IEEE/CVF International Conference on Computer Vision*, pp. 5799–5809, 2021.

Eric R Chan, Connor Z Lin, Matthew A Chan, Koki Nagano, Boxiao Pan, Shalini De Mello, Orazio Gallo, Leonidas J Guibas, Jonathan Tremblay, Sameh Khamis, Tero Karras, and Gordon Wetzstein. Efficient Geometry-Aware 3D Generative Adversarial Networks. In *Proceedings of the IEEE/CVF Conference on Computer Vision and Pattern Recognition*, pp. 16123–16133, 2022.

Eric R Chan, Koki Nagano, Matthew A Chan, Alexander W Bergman, Jeong Joon Park, Axel Levy, Miika Aittala, Shalini De Mello, Tero Karras, and Gordon Wetzstein. Generative Novel View Synthesis with 3D-Aware Diffusion Models. In *Proceedings of the IEEE/CVF International Conference on Computer Vision*, pp. 4217–4229, 2023.

Angel X Chang, Thomas Funkhouser, Leonidas Guibas, Pat Hanrahan, Qixing Huang, Zimo Li, Silvio Savarese, Manolis Savva, Shuran Song, Hao Su, Jianxiong Xiao, Li Yi, and Fisher Yu. Shapenet: An Information-Rich 3D Model Repository. *arXiv preprint arXiv:1512.03012*, 2015.

Anpei Chen, Zexiang Xu, Fuqiang Zhao, Xiaoshuai Zhang, Fanbo Xiang, Jingyi Yu, and Hao Su. MVSNeRF: Fast Generalizable Radiance Field Reconstruction from Multi-View Stereo. In *Proceedings of the IEEE/CVF International Conference on Computer Vision*, pp. 14124–14133, 2021.

Anpei Chen, Zexiang Xu, Andreas Geiger, Jingyi Yu, and Hao Su. TensoRF: Tensorial Radiance Fields. In *European Conference on Computer Vision*, pp. 333–350. Springer, 2022.

Mark Chen, Alec Radford, Rewon Child, Jeffrey Wu, Heewoo Jun, David Luan, and Ilya Sutskever. Generative Pretraining from Pixels. In *International Conference on Machine Learning*, pp. 1691–1703. PMLR, 2020.

Julian Chibane, Aayush Bansal, Verica Lazova, and Gerard Pons-Moll. Stereo Radiance Fields (SRF): Learning View Synthesis for Sparse Views of Novel Scenes. In *Proceedings of the IEEE/CVF Conference on Computer Vision and Pattern Recognition*, pp. 7911–7920, 2021.

Jasmine Collins, Shubham Goel, Kenan Deng, Achleshwar Luthra, Leon Xu, Erhan Gundogdu, Xi Zhang, Tomas F Yago Vicente, Thomas Dideriksen, Himanshu Arora, Matthieu Guillaumin, and Jitendra Malik. ABO: Dataset and Benchmarks for Real-World 3D Object Understanding. In *Proceedings of the IEEE/CVF Conference on Computer Vision and Pattern Recognition*, pp. 21126–21136, 2022.

Matt Deitke, Dustin Schwenk, Jordi Salvador, Luca Weihs, Oscar Michel, Eli VanderBilt, Ludwig Schmidt, Kiana Ehsani, Aniruddha Kembhavi, and Ali Farhadi. Objaverse: A Universe of Annotated 3D Objects. In *Proceedings of the IEEE/CVF Conference on Computer Vision and Pattern Recognition*, pp. 13142–13153, 2023.

Congyue Deng, Chiyu Jiang, Charles R Qi, Xinchen Yan, Yin Zhou, Leonidas Guibas, and Dragomir Anguelov. NeRDi: Single-View NeRF Synthesis with Language-Guided Diffusion as General Image Priors. In *Proceedings of the IEEE/CVF Conference on Computer Vision and Pattern Recognition*, pp. 20637–20647, 2023.

Laura Downs, Anthony Francis, Nate Koenig, Brandon Kinman, Ryan Hickman, Krista Reymann, Thomas B McHugh, and Vincent Vanhoucke. Google Scanned Objects: A High-Quality Dataset of 3D Scanned Household Items. In *International Conference on Robotics and Automation*, pp. 2553–2560. IEEE, 2022.

Patrick Esser, Robin Rombach, and Bjorn Ommer. Taming Transformers for High-Resolution Image Synthesis. In *Proceedings of the IEEE/CVF Conference on Computer Vision and Pattern Recognition*, pp. 12873–12883, 2021.

Sara Fridovich-Keil, Alex Yu, Matthew Tancik, Qinhong Chen, Benjamin Recht, and Angjoo Kanazawa. Plenoxels: Radiance Fields without Neural Networks. In *Proceedings of the IEEE/CVF Conference on Computer Vision and Pattern Recognition*, pp. 5501–5510, 2022.

Matheus Gadelha, Subhransu Maji, and Rui Wang. 3D Shape Induction from 2D Views of Multiple Objects. In *International Conference on 3D Vision*, pp. 402–411. IEEE, 2017.

Ian Goodfellow, Jean Pouget-Abadie, Mehdi Mirza, Bing Xu, David Warde-Farley, Sherjil Ozair, Aaron Courville, and Yoshua Bengio. Generative Adversarial Nets. *Advances in Neural Information Processing Systems*, 28, 2014.

Jiatao Gu, Yuyang Wang, Yizhe Zhang, Qihang Zhang, Dinghuai Zhang, Navdeep Jaitly, Josh Susskind, and Shuangfei Zhai. DART: Denoising Autoregressive Transformer for Scalable Text-to-Image Generation. *arXiv preprint arXiv:2410.08159*, 2024.

Jian Han, Jinlai Liu, Yi Jiang, Bin Yan, Yuqi Zhang, Zehuan Yuan, Bingyue Peng, and Xiaobing Liu. Infinity: Scaling Bitwise Autoregressive Modeling for High-Resolution Image Synthesis. *arXiv preprint arXiv:2412.04431*, 2024.

Tom Henighan, Jared Kaplan, Mor Katz, Mark Chen, Christopher Hesse, Jacob Jackson, Heewoo Jun, Tom B Brown, Prafulla Dhariwal, Scott Gray, Chris Hallacy, Benjamin Mann, Alec Radford, Aditya Ramesh, Nick Ryder, Daniel M Ziegler, John Schulman, Dario Amodei, and Sam McCandlish. Scaling Laws for Autoregressive Generative Modeling. *arXiv preprint arXiv:2010.14701*, 2020.

Jonathan Ho and Tim Salimans. Classifier-Free Diffusion Guidance. *NeurIPS Workshop on Deep Generative Models and Downstream Applications*, 2021.

Yicong Hong, Kai Zhang, Jiuxiang Gu, Sai Bi, Yang Zhou, Difan Liu, Feng Liu, Kalyan Sunkavalli, Trung Bui, and Hao Tan. LRM: Large Reconstruction Model for Single Image to 3D. In *International Conference on Learning Representations*, 2024.

Binbin Huang, Zehao Yu, Anpei Chen, Andreas Geiger, and Shenghua Gao. 2D Gaussian Splatting for Geometrically Accurate Radiance Fields. In *ACM SIGGRAPH*, pp. 1–11, 2024.

Ajay Jain, Matthew Tancik, and Pieter Abbeel. Putting NeRF on a Diet: Semantically Consistent Few-Shot View Synthesis. In *Proceedings of the IEEE/CVF International Conference on Computer Vision*, pp. 5885–5894, 2021.

Haian Jin, Hanwen Jiang, Hao Tan, Kai Zhang, Sai Bi, Tianyuan Zhang, Fujun Luan, Noah Snavely, and Zexiang Xu. LVSM: A Large View Synthesis Model with Minimal 3D Inductive Bias. In *International Conference on Learning Representations*, 2025.

Jared Kaplan, Sam McCandlish, Tom Henighan, Tom B Brown, Benjamin Chess, Rewon Child, Scott Gray, Alec Radford, Jeffrey Wu, and Dario Amodei. Scaling Laws for Neural Language Models. *arXiv preprint arXiv:2001.08361*, 2020.

Chris Kelly, Luhui Hu, Bang Yang, Yu Tian, Deshun Yang, Cindy Yang, Zaoshan Huang, Zihao Li, Jiayin Hu, and Yuexian Zou. VisionGPT: Vision-Language Understanding Agent Using Generalized Multimodal Framework. *arXiv preprint arXiv:2403.09027*, 2024.

Bernhard Kerbl, Georgios Kopanas, Thomas Leimkühler, and George Drettakis. 3D Gaussian Splatting for Real-Time Radiance Field Rendering. *ACM Transactions on Graphics*, 42(4):139–1, 2023.

Dan Kondratyuk, Lijun Yu, Xiuye Gu, José Lezama, Jonathan Huang, Grant Schindler, Rachel Hornung, Vighnesh Birodkar, Jimmy Yan, Ming-Chang Chiu, Krishna Somandepalli, Hassan Akbari, Yair Alon, Yong Cheng, Josh Dillon, Agrim Gupta, Meera Hahn, Anja Hauth, David Hendon, Alonso Martinex, David Minnen, Mikhail Sirotenko, Kihyuk Sohn, Xuan Yang, Hartwig Adam, Ming-Hsuan Yang, Irfan Essa, Huisheng Wang, David A Ross, and Bryan Seybold. Videopoet: A Large Language Model for Zero-Shot Video Generation. In *International Conference on Machine Learning*. PMLR, 2024.

Xin Kong, Shikun Liu, Xiaoyang Lyu, Marwan Taher, Xiaojuan Qi, and Andrew J Davison. EscherNet: A Generative Model for Scalable View Synthesis. In *Proceedings of the IEEE/CVF Conference on Computer Vision and Pattern Recognition*, pp. 9503–9513, 2024.

Xin Kong, Daniel Watson, Yannick Strümpler, Michael Niemeyer, and Federico Tombari. CausNVS: Autoregressive Multi-view Diffusion for Flexible 3D Novel View Synthesis. *arXiv preprint arXiv:2509.06579*, 2025.

Jonáš Kulhánek, Erik Derner, Torsten Sattler, and Robert Babuška. Viewformer: Nerf-Free Neural Rendering from Few Images using Transformers. In *European Conference on Computer Vision*, pp. 198–216. Springer, 2022.

Alina Kuznetsova, Hassan Rom, Neil Alldrin, Jasper Uijlings, Ivan Krasin, Jordi Pont-Tuset, Shahab Kamali, Stefan Popov, Matteo Malloci, Alexander Kolesnikov, Tom Duerig, and Vittorio Ferrari. The Open Images Dataset v4: Unified Image Classification, Object Detection, and Visual Relationship Detection at Scale. *International Journal of Computer Vision*, 128(7):1956–1981, 2020.

Doyup Lee, Chiheon Kim, Saehoon Kim, Minsu Cho, and Wook-Shin Han. Autoregressive Image Generation Using Residual Quantization. In *Proceedings of the IEEE/CVF Conference on Computer Vision and Pattern Recognition*, pp. 11523–11532, 2022.

Xiang Li, Kai Qiu, Hao Chen, Jason Kuen, Zhe Lin, Rita Singh, and Bhiksha Raj. ControlVAR: Exploring Controllable Visual Autoregressive Modeling. *arXiv preprint arXiv:2406.09750*, 2024.

Zongming Li, Tianheng Cheng, Shoufa Chen, Peize Sun, Haocheng Shen, Longjin Ran, Xiaoxin Chen, Wenyu Liu, and Xinggang Wang. ControlAR: Controllable Image Generation with Autoregressive Models. In *International Conference on Learning Representations*, 2025.

Ruoshi Liu, Rundi Wu, Basile Van Hoorick, Pavel Tokmakov, Sergey Zakharov, and Carl Vondrick. Zero-1-to-3: Zero-Shot One Image to 3D Object. In *Proceedings of the IEEE/CVF International Conference on Computer Vision*, pp. 9298–9309, 2023.

Yuan Liu, Cheng Lin, Zijiao Zeng, Xiaoxiao Long, Lingjie Liu, Taku Komura, and Wenping Wang. SyncDreamer: Generating Multiview-Consistent Images from a Single-View Image. In *International Conference on Learning Representations*, 2024.

Ilya Loshchilov and Frank Hutter. Decoupled Weight Decay Regularization. In *International Conference on Learning Representations*, 2019.

Taiming Lu, Tianmin Shu, Junfei Xiao, Luoxin Ye, Jiahao Wang, Cheng Peng, Chen Wei, Daniel Khashabi, Rama Chellappa, Alan Yuille, and Jieneng Chen. GenEx: Generating an Explorable World. *arXiv preprint arXiv:2412.09624*, 2024.

Xiaoxiao Ma, Mohan Zhou, Tao Liang, Yalong Bai, Tiejun Zhao, Huaian Chen, and Yi Jin. STAR: Scale-Wise Text-to-Image Generation via Auto-Regressive Representations. *arXiv preprint arXiv:2406.10797*, 2024.

Alexander Mai, Peter Hedman, George Kopanas, Dor Verbin, David Futschik, Qiangeng Xu, Falko Kuester, Jonathan T Barron, and Yinda Zhang. EVER: Exact Volumetric Ellipsoid Rendering for Real-Time View Synthesis. *arXiv preprint arXiv:2410.01804*, 2024.

Luke Melas-Kyriazi, Iro Laina, Christian Rupprecht, and Andrea Vedaldi. RealFusion: 360º Reconstruction of Any Object from a Single Image. In *Proceedings of the IEEE/CVF Conference on Computer Vision and Pattern Recognition*, pp. 8446–8455, 2023.

Ben Mildenhall, Pratul P Srinivasan, Matthew Tancik, Jonathan T Barron, Ravi Ramamoorthi, and Ren Ng. NeRF: Representing Scenes as Neural Radiance Fields for View Synthesis. *Communications of the ACM*, 65(1):99–106, 2021.

Thomas Müller, Alex Evans, Christoph Schied, and Alexander Keller. Instant Neural Graphics Primitives with a Multiresolution Hash Encoding. *ACM Transactions on Graphics*, 41(4):1–15, 2022.

Nithin Gopalakrishnan Nair, Srinivas Kaza, Xuan Luo, Vishal M Patel, Stephen Lombardi, and Jungyeon Park. Scaling Transformer-Based Novel View Synthesis Models with Token Disentanglement and Synthetic Data. *arXiv preprint arXiv:2509.06950*, 2025.

Thu Nguyen-Phuoc, Chuan Li, Lucas Theis, Christian Richardt, and Yong-Liang Yang. HoloGAN: Unsupervised Learning of 3D Representations from Natural Images. In *Proceedings of the IEEE/CVF International Conference on Computer Vision*, pp. 7588–7597, 2019.

Michael Niemeyer and Andreas Geiger. GIRAFFE: Representing Scenes as Compositional Generative Neural Feature Fields. In *Proceedings of the IEEE/CVF Conference on Computer Vision and Pattern Recognition*, pp. 11453–11464, 2021.

Michael Niemeyer, Jonathan T Barron, Ben Mildenhall, Mehdi SM Sajjadi, Andreas Geiger, and Noha Radwan. RegNeRF: Regularizing Neural Radiance Fields for View Synthesis from Sparse Inputs. In *Proceedings of the IEEE/CVF Conference on Computer Vision and Pattern Recognition*, pp. 5480–5490, 2022.

OpenAI. DALL-E Mini Model Card, 2022. https://huggingface.co/dalle-mini/dalle-mini.

OpenAI. GPT-4V(ision) System Card, 2023. https://openai.com/index/gpt-4v-system-card.

Niki Parmar, Ashish Vaswani, Jakob Uszkoreit, Lukasz Kaiser, Noam Shazeer, Alexander Ku, and Dustin Tran. Image Transformer. In *International Conference on Machine Learning*, pp. 4055–4064. PMLR, 2018.

Adam Paszke, Sam Gross, Francisco Massa, Adam Lerer, James Bradbury, Gregory Chanan, Trevor Killeen, Zeming Lin, Natalia Gimelshein, Luca Antiga, Alban Desmaison, Andreas Köpf, Edward Yang, Zach DeVito, Martin Raison, Alykhan Tejani, Sasank Chilamkurthy, Benoit Steiner, Lu Fang, Junjie Bai, and Soumith Chintala. PyTorch: An Imperative Style, High-Performance Deep Learning Library. *Advances in Neural Information Processing Systems*, 33, 2019.

William Peebles and Saining Xie. Scalable Diffusion Models with Transformers. In *Proceedings of the IEEE/CVF International Conference on Computer Vision*, pp. 4195–4205, 2023.

Justin Pinkney. Stable Diffusion Image Variations, 2023. https://www.justinpinkney.com/blog/2023/stable-diffusion-image-variations.

Reiner Pope, Sholto Douglas, Aakanksha Chowdhery, Jacob Devlin, James Bradbury, Jonathan Heek, Kefan Xiao, Shivani Agrawal, and Jeff Dean. Efficiently Scaling Transformer Inference. *Proceedings of Machine Learning and Systems*, 5:606–624, 2023.

Alec Radford, Karthik Narasimhan, Tim Salimans, and Ilya Sutskever. Improving Language Understanding by Generative Pre-Training, 2018. https://openai.com/index/language-unsupervised.

Alec Radford, Jeffrey Wu, Rewon Child, David Luan, Dario Amodei, and Ilya Sutskever. Language Models are Unsupervised Multitask Learners. *OpenAI Blog*, 1(8):9, 2019.

Alec Radford, Jong Wook Kim, Chris Hallacy, Aditya Ramesh, Gabriel Goh, Sandhini Agarwal, Girish Sastry, Amanda Askell, Pamela Mishkin, Jack Clark, Gretchen Krueger, and Ilya Sutskever. Learning Transferable Visual Models from Natural Language Supervision. In *International Conference on Machine Learning*, pp. 8748–8763. PMLR, 2021.

Aditya Ramesh, Mikhail Pavlov, Gabriel Goh, Scott Gray, Chelsea Voss, Alec Radford, Mark Chen, and Ilya Sutskever. Zero-Shot Text-to-Image Generation. In *International Conference on Machine Learning*, pp. 8821–8831. PMLR, 2021.

Ali Razavi, Aaron Van den Oord, and Oriol Vinyals. Generating Diverse High-Fidelity Images with VQ-VAE-2. *Advances in Neural Information Processing Systems*, 33, 2019.

Sucheng Ren, Qihang Yu, Ju He, Xiaohui Shen, Alan Yuille, and Liang-Chieh Chen. FlowAR: Scale-Wise Autoregressive Image Generation Meets Flow Matching. *arXiv preprint arXiv:2412.15205*, 2024a.

Sucheng Ren, Yaodong Yu, Nataniel Ruiz, Feng Wang, Alan Yuille, and Cihang Xie. M-VAR: Decoupled Scale-wise Autoregressive Modeling for High-Quality Image Generation. *arXiv preprint arXiv:2411.10433*, 2024b.

Robin Rombach, Patrick Esser, and Björn Ommer. Geometry-Free View Synthesis: Transformers and no 3D Priors. In *Proceedings of the IEEE/CVF International Conference on Computer Vision*, pp. 14356–14366, 2021.

Robin Rombach, Andreas Blattmann, Dominik Lorenz, Patrick Esser, and Björn Ommer. High-Resolution Image Synthesis with Latent Diffusion Models. In *Proceedings of the IEEE/CVF Conference on Computer Vision and Pattern Recognition*, pp. 10684–10695, 2022.

Mehdi SM Sajjadi, Henning Meyer, Etienne Pot, Urs Bergmann, Klaus Greff, Noha Radwan, Suhani Vora, Mario Lučić, Daniel Duckworth, Alexey Dosovitskiy, Jakob Uszkoreit, Thomas Funkhouser, and Andrea Tagliasacchi. Scene Representation Transformer: Geometry-Free Novel View Synthesis through Set-Latent Scene Representations. In *Proceedings of the IEEE/CVF Conference on Computer Vision and Pattern Recognition*, pp. 6229–6238, 2022.

Kyle Sargent, Zizhang Li, Tanmay Shah, Charles Herrmann, Hong-Xing Yu, Yunzhi Zhang, Eric Ryan Chan, Dmitry Lagun, Li Fei-Fei, Deqing Sun, and Jiajun Wu. ZeroNVS: Zero-Shot 360-Degree View Synthesis from a Single Real Image. In *Proceedings of the IEEE/CVF Conference on Computer Vision and Pattern Recognition*, pp. 9420–9429, 2024.

Christoph Schuhmann, Romain Beaumont, Richard Vencu, Cade Gordon, Ross Wightman, Mehdi Cherti, Theo Coombes, Aarush Katta, Clayton Mullis, Mitchell Wortsman, Patrick Schramowski, Srivatsa Kundurthy, Katherine Crowson, Ludwig Schmidt, Robert Kaczmarczyk, and Jenia Jitsec. LAION-5B: An Open Large-Scale Dataset for Training Next Generation Image-Text Models. *Advances in Neural Information Processing Systems*, 36:25278–25294, 2022.

Katja Schwarz, Axel Sauer, Michael Niemeyer, Yiyi Liao, and Andreas Geiger. VoxGRAF: Fast 3D-Aware Image Synthesis with Sparse Voxel Grids. *Advances in Neural Information Processing Systems*, 36:33999–34011, 2022.

Ruoxi Shi, Hansheng Chen, Zhuoyang Zhang, Minghua Liu, Chao Xu, Xinyue Wei, Linghao Chen, Chong Zeng, and Hao Su. Zero123++: A Single Image to Consistent Multi-View Diffusion Base Model. *arXiv preprint arXiv:2310.15110*, 2023.

Cheng Sun, Min Sun, and Hwann-Tzong Chen. Direct Voxel Grid Optimization: Super-Fast Convergence for Radiance Fields Reconstruction. In *Proceedings of the IEEE/CVF Conference on Computer Vision and Pattern Recognition*, pp. 5459–5469, 2022.

Quan Sun, Qiying Yu, Yufeng Cui, Fan Zhang, Xiaosong Zhang, Yueze Wang, Hongcheng Gao, Jingjing Liu, Tiejun Huang, and Xinlong Wang. Emu: Generative Pretraining in Multimodality. In *International Conference on Learning Representations*, 2023.

Haotian Tang, Yecheng Wu, Shang Yang, Enze Xie, Junsong Chen, Junyu Chen, Zhuoyang Zhang, Han Cai, Yao Lu, and Song Han. HART: Efficient Visual Generation with Hybrid Autoregressive Transformer. In *International Conference on Learning Representations*, 2025.

Jiaxiang Tang, Zhaoxi Chen, Xiaokang Chen, Tengfei Wang, Gang Zeng, and Ziwei Liu. LGM: Large Multi-View Gaussian Model for High-Resolution 3D Content Creation. In *European Conference on Computer Vision*. Springer, 2024.

Keyu Tian, Yi Jiang, Zehuan Yuan, Bingyue Peng, and Liwei Wang. Visual Autoregressive Modeling: Scalable Image Generation via Next-Scale Prediction. *Advances in Neural Information Processing Systems*, 38, 2024.

Hugo Touvron, Thibaut Lavril, Gautier Izacard, Xavier Martinet, Marie-Anne Lachaux, Timothée Lacroix, Baptiste Rozière, Naman Goyal, Eric Hambro, Faisal Azhar, et al. Llama: Open and Efficient Foundation Language Models. *arXiv preprint arXiv:2302.13971*, 2023.

Jonathan Tremblay, Moustafa Meshry, Alex Evans, Jan Kautz, Alexander Keller, Sameh Khamis, Thomas Müller, Charles Loop, Nathan Morrical, Koki Nagano, et al. Rtmv: A ray-traced multi-view synthetic dataset for novel view synthesis. *arXiv preprint arXiv:2205.07058*, 2022.

Yuanpeng Tu, Hao Luo, Xi Chen, Sihui Ji, Xiang Bai, and Hengshuang Zhao. VideoAnydoor: High-Fidelity Video Object Insertion with Precise Motion Control. *arXiv preprint arXiv:2501.01427*, 2025.

Aaron Van Den Oord, Oriol Vinyals, and Koray Kavukcuoglu. Neural Discrete Representation Learning. *Advances in Neural Information Processing Systems*, 31, 2017.

Ashish Vaswani, Noam Shazeer, Niki Parmar, Jakob Uszkoreit, Llion Jones, Aidan Gomez, Lukasz Kaiser, and Illia Polosukhin. Attention is All You Need. *Advances in Neural Information Processing Systems*, 31, 2017.

Guangcong Wang, Zhaoxi Chen, Chen Change Loy, and Ziwei Liu. SparseNeRF: Distilling Depth Ranking for Few-Shot Novel View Synthesis. In *Proceedings of the IEEE/CVF International Conference on Computer Vision*, pp. 9065–9076, 2023.

Daniel Watson, William Chan, Ricardo Martin-Brualla, Jonathan Ho, Andrea Tagliasacchi, and Mohammad Norouzi. Novel View Synthesis with Diffusion Models. In *International Conference on Learning Representations*, 2023.

Daniel Watson, William Chan, Ricardo Martin-Brualla, Jonathan Ho, Andrea Tagliasacchi, and Mohammad Norouzi. Consistent123: Improve Consistency for One Image to 3D Object Synthesis. In *International Conference on Learning Representations*, 2024.

Chenfei Wu, Jian Liang, Lei Ji, Fan Yang, Yuejian Fang, Daxin Jiang, and Nan Duan. NÜWA: Visual Synthesis Pre-training for Neural visUal World creAtion. In *European Conference on Computer Vision*, pp. 720–736. Springer, 2022.

Rundi Wu, Ben Mildenhall, Philipp Henzler, Keunhong Park, Ruiqi Gao, Daniel Watson, Pratul P Srinivasan, Dor Verbin, Jonathan T Barron, Ben Poole, and Aleksander Holyński. ReconFusion: 3D Reconstruction with Diffusion Priors. In *Proceedings of the IEEE/CVF Conference on Computer Vision and Pattern Recognition*, pp. 21551–21561, 2024.

Tong Wu, Jiarui Zhang, Xiao Fu, Yuxin Wang, Jiawei Ren, Liang Pan, Wayne Wu, Lei Yang, Jiaqi Wang, Chen Qian, Dahua Lin, and Ziwei Liu. Omniobject3d: Large-vocabulary 3d object dataset for realistic perception, reconstruction and generation. In *Proceedings of the IEEE/CVF Conference on Computer Vision and Pattern Recognition*, pp. 803–814, 2023.

Jianfeng Xiang, Zelong Lv, Sicheng Xu, Yu Deng, Ruicheng Wang, Bowen Zhang, Dong Chen, Xin Tong, and Jiaolong Yang. Structured 3D Latents for Scalable and Versatile 3D Generation. In *Proceedings of the IEEE/CVF Conference on Computer Vision and Pattern Recognition*, pp. 21469–21480, 2025.

Dejia Xu, Yifan Jiang, Peihao Wang, Zhiwen Fan, Humphrey Shi, and Zhangyang Wang. SinNeRF: Training Neural Radiance Fields on Complex Scenes from a Single Image. In *European Conference on Computer Vision*, pp. 736–753. Springer, 2022.

Wilson Yan, Yunzhi Zhang, Pieter Abbeel, and Aravind Srinivas. VideoGPT: Video Generation Using VQ-VAE and Transformers. *arXiv preprint arXiv:2104.10157*, 2021.

Ziyu Yao, Jialin Li, Yifeng Zhou, Yong Liu, Xi Jiang, Chengjie Wang, Feng Zheng, Yuexian Zou, and Lei Li. CAR: Controllable Autoregressive Modeling for Visual Generation. *arXiv preprint arXiv:2410.04671*, 2024.

Jianglong Ye, Peng Wang, Kejie Li, Yichun Shi, and Heng Wang. Consistent-1-to-3: Consistent Image to 3D View Synthesis via Geometry-Aware Diffusion Models. In *International Conference on 3D Vision*, pp. 664–674. IEEE, 2024.

Alex Yu, Ruilong Li, Matthew Tancik, Hao Li, Ren Ng, and Angjoo Kanazawa. Plenoctrees for Real-Time Rendering of Neural Radiance Fields. In *Proceedings of the IEEE/CVF International Conference on Computer Vision*, pp. 5752–5761, 2021a.

Alex Yu, Vickie Ye, Matthew Tancik, and Angjoo Kanazawa. PixelNeRF: Neural Radiance Fields from One or Few Images. In *Proceedings of the IEEE/CVF Conference on Computer Vision and Pattern Recognition*, pp. 4578–4587, 2021b.

Jiahui Yu, Xin Li, Jing Yu Koh, Han Zhang, Ruoming Pang, James Qin, Alexander Ku, Yuanzhong Xu, Jason Baldridge, and Yonghui Wu. Vector-Quantized Image Modeling with Improved VQGAN. In *International Conference on Learning Representations*, 2022a.

Jiahui Yu, Yuanzhong Xu, Jing Yu Koh, Thang Luong, Gunjan Baid, Zirui Wang, Vijay Vasudevan, Alexander Ku, Yinfei Yang, Burcu Karagol Ayan, Ben Hutchinson, Wei Han, Zarana Parekh, Xin Li, Han Zhang, Jason Baldridge, and Yonghui Wu. Scaling Autoregressive Models for Content-Rich Text-to-Image Generation. *Transactions on Machine Learning Research*, 2022b.

Kai Zhang, Sai Bi, Hao Tan, Yuanbo Xiangli, Nanxuan Zhao, Kalyan Sunkavalli, and Zexiang Xu. GS-LRM: Large Reconstruction Model for 3D Gaussian Splatting. In *European Conference on Computer Vision*, pp. 1–19. Springer, 2025.

Lvmin Zhang, Anyi Rao, and Maneesh Agrawala. Adding Conditional Control to Text-to-Image Diffusion Models. In *Proceedings of the IEEE/CVF International Conference on Computer Vision*, pp. 3836–3847, 2023.

Chuanxia Zheng and Andrea Vedaldi. Free3D: Consistent Novel View Synthesis without 3D Representation. In *Proceedings of the IEEE/CVF Conference on Computer Vision and Pattern Recognition*, pp. 9720–9731, 2024.

Table 3: **Specifications for the checkpoints of varying sizes we trained.**

Depth	12	16	20	24	30
# of Parameters	135M	311M	601M	1.0B	2.0B
Training Time (h)	14.5	17.1	23.5	30.0	51.3
Inference Time (ms)	160	180	200	220	260

A Improving NVS Benchmarking

We notice that benchmarking in previous works have usually inherited the evaluation rendering settings used by Zero 1-to-3 (Liu et al., 2023). However, in this "classic" setting, we notice that input views are selected from a narrow range of elevation angles, which makes the task much easier but does not demonstrate the model's robustness across a wide range of possible views of an object. This is also a discrepancy with the training setting, where camera poses are sampled across an entire viewing sphere (save for very high elevation angles, and with the radial distance varying).

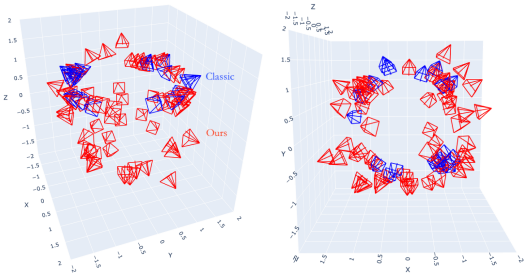

Figure 10: **Improving NVS evaluation.** A free view and a top view of the "classic" input camera views compared to ours (40 each sampled).

Hence, we choose to make the evaluation setting exactly the same as the training setting. A visual comparison between cameras sampled in our evaluation setting and the "classic" one is in Fig. 10. We note that this makes the task considerably more difficult (but the camera poses are still all within the training range, and hence are not out-of-distribution), and requires models to be more robust with respect to the input pose.

Regarding more details on the evaluation dataset, for all datasets except NeRF, we sample 100 objects randomly, and render 7 views for 3D objects (for RTMV we directly sample 7 views), with one being used as the input view and the other 6 being used for evaluation; for NeRF, we use all 8 objects, sample one random input view from each object's training set, and evaluate across all 200 testing views.

B Training Specifications

Optimization of our model is conducted via AdamW (Loshchilov & Hutter, 2019), and implementation uses PyTorch (Paszke et al., 2019). We trained on 32 NVIDIA H200 GPUs across four nodes on a server cluster, and tested inference speed on a single H200. We report baseline results from officially recommended default settings.

We trained each of our released checkpoint models for 100 epochs on the full Objaverse dataset (800k objects), with a base learning rate of 8×10^{-5} (result of grid search). We randomly render 12 views at 256×256 resolution from each object, and randomly select two as the input and target during each iteration. Information regarding training time and numbers of parameters are found in Tab. 3. During rendering, aligning with the common approach as in works like Liu et al. (2023), we randomly sample on a sphere with radius uniformly chosen from $[1.5, 2.2]$, and use the same setting for evaluation (as shown in Fig. 10).

C Backbone Architecture Details

Multi-Scale Tokenization The VQVAE contains an image encoder-decoder pair $(\mathcal{E}, \mathcal{D})$, a quantizer $\mathcal{Q}$, and a learnable codebook Z with vocabulary size V. The image encoder takes an image x as input and encodes it into a feature map $f = \mathcal{E}(x) \in \mathbb{R}^{h \times w \times C}$ (where h,w are the latent height/width, and C is the embedding dimension). Note that the latent dimensions of the image are based on patching, similar to conventional autoregression and latent diffusion. The feature maps are then quantized as $q = \mathcal{Q}(f) \in [1..V]^{h \times w}$. The quantizer does this by mapping each patch $f_{i,j}$ to the Euclidean nearest codebook entry Z_v:

$$q_{i,j} = \underset{v \in [1..V]}{\arg\min} ||Z_v - f_{i,j}||_2. \tag{4}$$

The key to the multi-scale formulation is that the input image is resized into different resolution scales. For instance, since we use 16×16 patches, the 3×3 scale would reshape the image to 48×48 pixel resolution before tokenization; and the corresponding scale token would contain 9 patch tokens. All scales share the same codebook Z, thus ensuring a consistent vocabulary is used across different token scales. The image can then be reconstructed using the decoder $\mathcal{D}$ given the quantized tokens.

Next-Scale Prediction Transformers Based on a frozen VQVAE the autoregressive model is formulated as follows. We attempt to achieve a probabilistic model p_θ (the next-scale transformer) conditioned by our inputs (x, R, T) such that the joint likelihood of scale tokens $(r_1, r_2, \cdots, r_K)$ representing the distribution of $x^*_{R,T}$ can be modeled as

$$g(x, R, T) = p_\theta(r_1, r_2, \cdots, r_K | x, R, T) = \prod_{k=1}^{K} p_\theta(r_k | x, R, T, r_1, r_2, \cdots, r_{k-1}). \tag{5}$$

Note that here the autoregressive assumption is that each scale r_k only depends on the conditioning and the previous scales (similar to a coarse-to-fine process), instead of the later scales. We add conditioning tokens c_k (as described in Sec. 3.4) as well for additional information.

We use teacher forcing to train the model, where $(r_1, r_2, \cdots, r_{K-1})$ of x^* and conditioning from x are used for causally predicting all tokens $(r_1, r_2, \cdots, r_K)$ of x^*. After sending inputs and conditioning through several transformer blocks, the eventual results are passed through a classifier head (consisting of a single linear layer) and outputted as classification logits, after which the cross-entropy loss between the logits and ground truths is taken for backpropagation.

Implementation-wise, each scale token r_k is first interpolated to the same size as r_{k+1} by taking the corresponding feature map f, resizing it accordingly, and applying tokenization. An exception is the $[s] \rightarrow r_1$ mapping, which does not require resizing. The upscaled results e_k are then taken as input to the causal transformer. Each attention layer uses adaptive layer normalization (AdaLN) (Peebles & Xie, 2023) conditioned by the start token (to ensure consistency with the global encoding conditioning) and multi-head self-attention (Vaswani et al., 2017). We refer to the number of AdaLN transformer blocks per prediction step as the model depth and the dimension of tokens C as the model width. For easy scaling, in our experiments we set the model width to always be 64 times the depth.

During inference, we first find c_k and the start token $[s]$ using x. We then use them to infer the distribution of r_1 and sample from the distribution. We then use the available information to infer r_2, and so on. Note that already known tokens are kv-cached (Pope et al., 2023) and not replaced in further inference steps. The final inferred r_k values are passed through the VQVAE decoder to arrive at $\hat{x}^*$.